

RESEARCH

Open Access



Neuregulin-1 inhibits CoCl₂-induced upregulation of excitatory amino acid carrier 1 expression and oxidative stress in SH-SY5Y cells and the hippocampus of mice

Han-Byeol Kim^{1†}, Ji-Young Yoo^{1†}, Seung-Yeon Yoo^{1†}, Jun-Ho Lee², Wonseok Chang³, Hye-Sun Kim^{4,5}, Tai-Kyoung Baik^{1*} and Ran-Sook Woo^{1*} 

Abstract

Excitatory amino acid carrier 1 (EAAC1) is an important subtype of excitatory amino acid transporters (EAATs) and is the route for neuronal cysteine uptake. CoCl₂ is not only a hypoxia-mimetic reagent but also an oxidative stress inducer. Here, we found that CoCl₂ induced significant EAAC1 overexpression in SH-SY5Y cells and the hippocampus of mice. Transient transfection of EAAC1 reduced CoCl₂-induced cytotoxicity in SH-SY5Y cells. Based on this result, upregulation of EAAC1 expression by CoCl₂ is thought to represent a compensatory response against oxidative stress in an acute hypoxic state. We further demonstrated that pretreatment with Neuregulin-1 (NRG1) rescued CoCl₂-induced upregulation of EAAC1 and tau expression. NRG1 plays a protective role in the CoCl₂-induced accumulation of reactive oxygen species (ROS) and reduction in antioxidative enzyme (SOD and GPx) activity. Moreover, NRG1 attenuated CoCl₂-induced apoptosis and cell death. NRG1 inhibited the CoCl₂-induced release of cleaved caspase-3 and reduction in Bcl-X_L levels. Our novel finding suggests that NRG1 may play a protective role in hypoxia through the inhibition of oxidative stress and thereby maintain normal EAAC1 expression levels.

Keywords: CoCl₂, EAAC1, Neuregulin-1, Oxidative stress, Apoptosis

Introduction

Excitatory amino acid carrier 1 (EAAC1, also referred to as EAAT3) is one neuronal subtype of excitatory amino acid transporter (EAAT) that is ubiquitously expressed in the central nervous system (CNS). EAAC1 can also transport cysteine at a rate comparable to that of glutamate and is the primary route for the uptake of neuronal cysteine. Cysteine is a critically important substrate

for the synthesis of glutathione (GSH), one of the most important intracellular antioxidants in the brain [1, 2]. Mature neurons utilize cysteine but not cystine for GSH synthesis [3, 4]. EAAC1-mediated uptake may be the major source of cysteine for GSH synthesis in mature neurons [5]. Oxidative stress is a general premonitory hallmark of numerous brain pathologies and largely contributes to the acute and chronic outcomes of CNS disorders, such as epilepsy, ischemic stroke, amyotrophic lateral sclerosis, Alzheimer's disease and Parkinson's disease [6]. Modulation of EAAC1 activity correlates with neuronal GSH levels [7]. Knockdown of EAAC1 reduces cysteine uptake and intracellular GSH levels [8].

The intracellular response to hypoxia is regulated by hypoxia inducible factor-1 (HIF-1). HIF-1 is a

*Correspondence: tkbaik@eulji.ac.kr; rswoo@eulji.ac.kr

[†]Han-Byeol Kim, Ji-Young Yoo and Seung-Yeon Yoo contributed equally to this work

¹ Department of Anatomy and Neuroscience, College of Medicine, Eulji University, 143-5Jung-Gu, Yongdu-Dong, Daejeon 301-746, Republic of Korea

Full list of author information is available at the end of the article



transcription factor, and a heterodimer consisting of an oxygen-dependent regulatory HIF-1 α subunit and a constitutively expressed HIF-1 β subunit that acts as a master regulator of adaptation to a low oxygen environment in the cell [9]. Recent evidence suggests that the ROS produced in the mitochondria mediate HIF-1 α stabilization during hypoxia [9]. Hypoxia leads to a rapid increase in spontaneous vesicular glutamate release [10] and impaired glutamate uptake [11–13]. EAAC1 was increased at the transcript level in C6 cells by hypoxia [14]. Oxygen–glucose deprivation (OGD) induced the protein expression of EAAC1 in pure and mixed neuronal cultures and promoted EAAT3 activity, which increased glutamate uptake into cultured neurons [15]. EAAC1 transcript levels were transiently upregulated during the reperfusion phase in ischemia–reperfusion models [15]. Ischemia–reperfusion leads to oxidative stress and an accompanying transient increase in EAAT3 immunoreactivity in the hippocampus [16].

Neuregulin-1 (NRG1) is a member of the NRG family of growth factors that play important roles in the developing and adult CNS [17]. Recently, accumulating evidence has collectively shown that NRG1 is a new regulator of injury and repair with multifaceted roles in neuroprotection, remyelination, and immunomodulation. NRG1 protects against a number of CNS pathological conditions, including ischemia, neurotrauma, and neurodegenerative diseases [18–21, 23]. Our recent work showed that NRG1 regulated hypoxia-inducible factors such as HIF-1 α and p53 [24]. NRG1/ErbB4 attenuates neuronal cell damage under OGD in primary hippocampal neurons [25]. These findings suggest a correlation between NRG1 dysfunction and CNS pathology. Therefore, NRG1 may be a potential therapeutic target in the recovery of function after CNS injury.

Herein, we used cobalt chloride (CoCl₂), a hypoxia mimic, to induce oxidative stress in SH-SY5Y cells. Cobalt stimulates reactive oxygen species (ROS) generation through a nonenzymatic, nonmitochondrial mechanism, and CoCl₂ treatment induces HIF-1 α accumulation [26].

Our study provides conclusive molecular evidence that CoCl₂ strongly induces EAAC1 expression in SH-SY5Y cells and hippocampus of mice. These acute changes may respond against reactive oxidative stress. NRG1 reduced the CoCl₂-induced oxidative and thereby rescue upregulation of EAAC1.

Materials and methods

Reagents and antibodies

Recombinant β -type NRG1 was purchased from ProSpec (East Brunswick, NJ, USA). Antibodies were obtained from Millipore Corporation (Chemicon, MA, USA)

(EAAT3 (EAAC1), MAB1587), Santa Cruz Biotechnology Inc. (Santa Cruz, CA, USA) (Bcl-X_L, sc-8392; p53, sc-126; β -actin, sc-47778), Novus Biologicals (Centennial, CO, USA) (HIF-1 α , NB100-131; Tau, NBP-25613), ThermoFisher scientific (Waltham, MA, USA) (Phospho-Tau (AT8), #MN1020), Mybiosource (San Diego, CA, USA) (Phospho-Tau (ser422), #A11008), and Cell Signaling Technology (CST, MA, USA) (Caspase 3, #9662 s; cleaved caspase 3, # 9661 s; EAAC1, #12,179; Myc-tag, #2276; HRP-conjugated anti-rabbit IgG, #7076 s; HRP-conjugated anti-mouse IgG, #7074 s). CoCl₂ (C8661) was purchased from Sigma-Aldrich (St. Louis, MO, USA).

Animals and stereotaxic surgery

C57BL/6 (male, 10 weeks old, 24–27 g) mice were obtained from a laboratory animal supplier (Samtako Bio Korea) and were housed in cages under standard laboratory conditions with a 12-h light/12-h dark cycle. A total of twenty animals were randomly allocated to the following four groups: saline (n=8), NRG1 (n=8), CoCl₂ (n=8), and CoCl₂ + NRG1 (n=8). Experiments with animals were approved by the Institutional Animal Care and Use Committee of Eulji University (EUIACUC 19–08). All surgical procedures and perfusions were performed under anaesthesia via intraperitoneal injection of ketamine (100 mg/kg) with Rompun (10 mg/kg). The animals were subjected to a unilateral lesion by placing them in a stereotaxic apparatus. CoCl₂ (25 mM) was delivered in the ventral hippocampus of the right hemisphere (coordinates from bregma: anterior/posterior – 3.3 mm, medial/lateral + 2.8 mm, dorsal/ventral – 4.0 mm). Each microinjection unit was attached to a 10- μ l Hamilton micro-litre syringe via a glass tube, and administration was controlled by the experimenter at a rate of 1 μ l (volume injected) over a period of approximately 2 min 30 s.

Cell culture and transfection

SH-SY5Y human neuroblastoma cells were purchased from the American Type Culture Collection (Manassas, VA, USA) and cultured in Dulbecco's modified Eagle's medium (Invitrogen, Carlsbad, CA, USA) containing 10% fetal bovine serum (FBS) and a penicillin–streptomycin–amphotericin B mixture (Invitrogen) at 37 °C in a humidified atmosphere containing 5% CO₂. When the cells grew sufficiently in 100 mm culture dishes (SPL Life Sciences, Gyeonggi-do, Korea), they were subcultured in 6-well or 96-well plates. SH-SY5Y cells were transiently transfected with either 4 μ g of plasmid pcDNA3.1 (Mock) or pcDNA3.1-EAAC1-myc and 10 μ l of Lipofectamine 2000 (Invitrogen) in 250 μ l of Opti-MEM without serum according to the manufacturer's instructions. Transient transfection efficiencies were confirmed by Western blot in SH-SY5Y cells.

Assessment of cell death

Cell death after CoCl_2 treatment was assessed by determining the release of lactate dehydrogenase (LDH) into the culture medium, thereby indicating a loss of membrane integrity. LDH activity was measured using a commercial kit (Cytotox 96 nonradioactive cytotoxicity assay kit, Promega, Madison, WI, USA) according to the manufacturer's protocol. The absorbance was measured at 490 nm using a VICTOR X3 multilabel plate reader (PerkinElmer, Shelton, USA).

TUNEL staining

In situ DNA fragmentation was assessed using a terminal deoxynucleotidyl transferase (TdT) dUTP nick end labeling (TUNEL) staining kit (Roche Diagnostics) according to the manufacturer's instructions. Images were captured after counterstaining with 10 μM 4',6-diamidino-2-phenylindole (DAPI; Invitrogen) for 30 min. The number of apoptotic cells was counted in five random fields using a Zeiss LSM 5 LIVE confocal microscope (Carl Zeiss AG, Oberkochen, Germany). The apoptotic cells are expressed as the percentage of TUNEL-positive cells in the total number of DAPI-stained cells.

ROS measurement

ROS generation in SH-SY5Y cells was analyzed using the dye 2',7'-dichlorodihydrofluorescein diacetate (DCFH-DA; Invitrogen, CA, USA). SH-SY5Y cells were washed three times with Dulbecco's phosphate-buffered saline (DPBS) and then incubated at 37 °C in DPBS containing 20 μM DCFH-DA for 30 min. Once inside the cells, DCFH-DA is hydrolyzed by esterase to form polar DCFH, which then interacts with ROS. Cells were subsequently washed three times with DPBS and visualized with a fluorescence microscope (EVOS M5000, Thermo Fisher Scientific, Eugene, OR, USA) at an excitation wavelength of 485 nm.

Glutathione peroxidase (GPx) activity assay

GPx activity was determined using a Biovision glutathione peroxidase activity assay kit (Cayman Chemical Company, MI, USA) according to the manufacturer's protocol. SH-SY5Y cells were homogenized on ice in cold assay buffer and then centrifuged at 10,000 $\times g$ for 15 min at 4 °C. Then, 50 μl of cell supernatant was added to a 96-well plate with 50 μl of assay buffer. The reaction mixture was added to each sample and incubated for 15 min to deplete all GSSG in the samples. Ten microliters of cumene hydroperoxide substrate was subsequently added to initiate the enzymatic reaction. The absorbance was immediately measured at a wavelength of 340 nm using

a VICTOR X3 multilabel plate reader (PerkinElmer, Shelton, USA). GPx activity was calculated using an NADPH standard curve.

Superoxide dismutase (SOD) activity assay

SOD activity was measured using a commercially available kit (Cayman Chemical Company, MI, USA) according to the manufacturer's protocol. SH-SY5Y cells were homogenized in cold 20 mM HEPES buffer (pH 7.2) and centrifuged at 1,500 $\times g$ for 5 min at 4 °C. Each sample (10 μl) was added to a 96-well plate with 200 μl of the diluted radical detector. Then, 20 μl of diluted xanthine oxidase was added to initiate the enzymatic reaction. The absorbance was immediately measured at a wavelength of 450 nm using a VICTOR X3 multilabel plate reader (PerkinElmer, Shelton, USA).

Immunofluorescence analysis

SH-SY5Y cells were fixed using 4% paraformaldehyde and 4% sucrose in DPBS (pH 7.4) for 20 min at room temperature (RT). Next, the cells were permeabilized and blocked using DPBS containing 1% BSA and 0.1% Triton X-100 at RT for 30 min, and then primary antibodies (mouse anti-EAAC1 (1:100) and rabbit anti-tau (1:100)) were added and incubated overnight at 4 °C. The cells were then washed three times in PBS and incubated with Alexa Fluor 488 goat anti-mouse IgG and Alexa Fluor 594 goat anti-chicken IgG (Jackson ImmunoResearch Laboratories, Inc., 1:200) for 2 h at RT. After counterstaining with DAPI (10 μM in DPBS), the cells were mounted in Vectorshield (Vector Laboratories). Fluorescent images were acquired with an LSM 5 LIVE confocal system (Carl Zeiss AG, Oberkochen, Germany).

Dihydroethidium (DHE) staining

To assess superoxide production, the brain was immediately frozen in embedding medium [22]. Briefly, post-fixed cryosections (15 μm) were incubated in DPBS containing 10 μM DHE (Invitrogen CA, USA) for 30 min at 37 °C in the dark room. The sections were then washed thrice with DPBS and mounted in Vectorshield (Vector Laboratories). Fluorescent images were acquired with an LSM 5 LIVE confocal system (Carl Zeiss AG, Oberkochen, Germany). Images were obtained using an excitation wavelength of 561 nm and an emission wavelength of 640 nm.

Western blot analysis

Western blotting was performed as previously described [23]. Briefly, tissues were homogenized using a modified homogenization buffer (50 mM Tris-HCl [pH 7.4], 150 mM NaCl, 1% NP-40, 0.25% sodium-deoxycholate, 1 mM PMSE, 1 mM EDTA, and 1 $\mu\text{g/ml}$ each of aprotinin,

leupeptin, and pepstatin protease inhibitors). Samples were then resolved using SDS-PAGE, transferred to nitrocellulose membranes and subsequently blocked with TBS containing 5% fat-free milk and 0.05% Tween-20 for 1 h. Next, the membranes were incubated overnight at 4 °C with primary antibodies (anti-EAAC1, 1:1,000, Millipore Corporation; anti-cleaved caspase-3, 1:1,000, anti-caspase 3, 1:1,000, anti-Myc-tag, 1:1,000, Cell Signaling; anti-HIF-1 α , 1:1,000, Novus Biologicals; anti-p53, 1:1,000, anti- β -actin, 1:5,000, Santa Cruz Biotechnology) and developed using horseradish peroxidase-conjugated secondary antibodies. Immunodetection was performed with a chemiluminescence system (Amersham Pharmacia) and a ChemiDoc TM tough imaging system (BioRad, California, USA).

Statistical analysis

The data are presented as the means \pm SEM of three or more independent experiments. Student's paired *t*-test was used for comparisons of the means between two groups of cells in a single experiment. For the data of more than two groups, statistical analyses were performed by one-way analysis of variance (ANOVA) followed by Bonferroni's post hoc test. A value of *P* < 0.05 was considered statistically significant.

Results

CoCl₂ increased EAAC1 protein expression in SH-SY5Y cells and the ventral hippocampus (VH) of mice

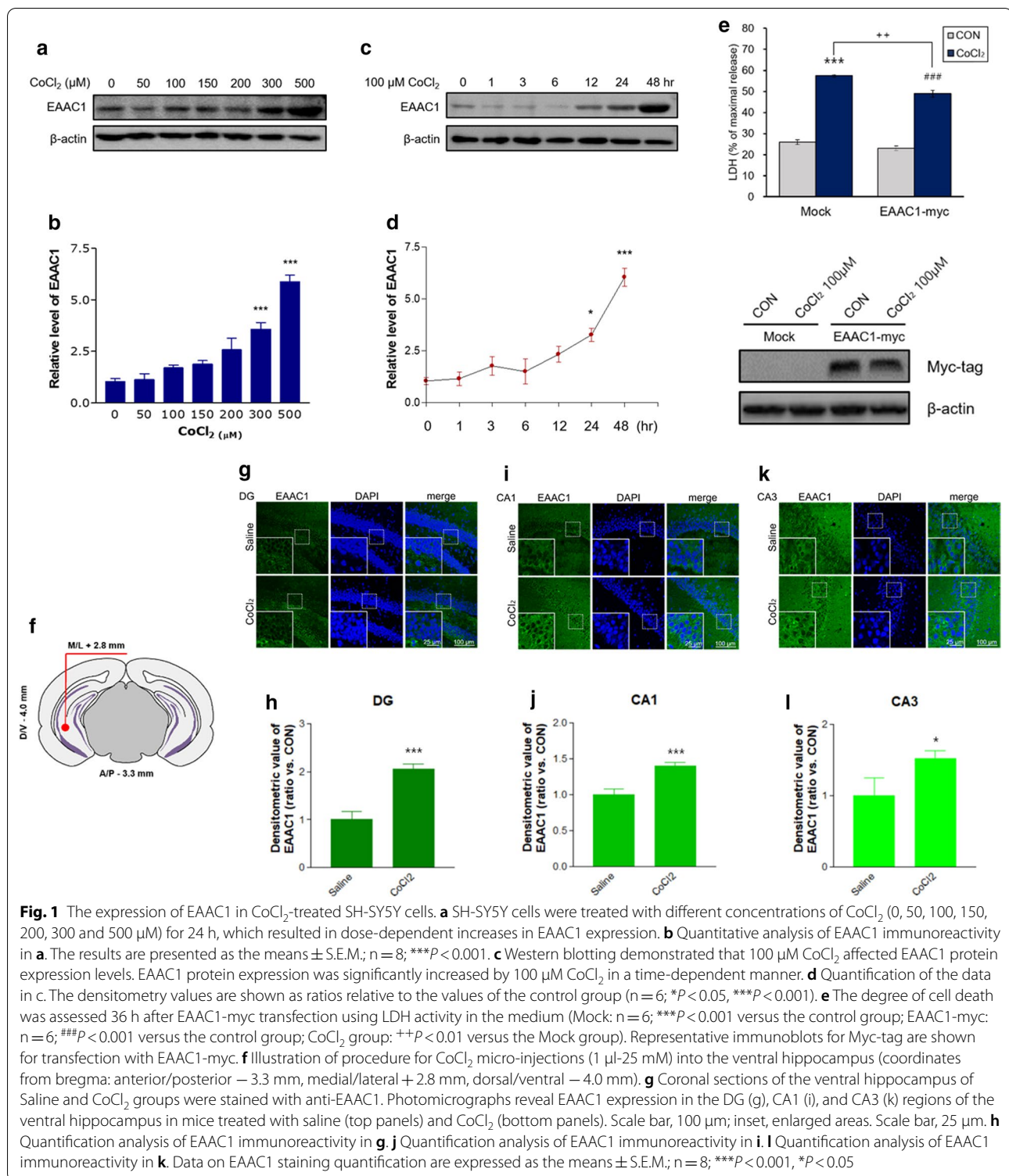
We used CoCl₂ to mimic hypoxia in SH-SY5Y cells. First, we examined whether CoCl₂ altered the protein levels of EAAC1 in SH-SY5Y cells. We found that there was a dose-dependent increase in EAAC1 expression after 24 h of CoCl₂ (50–500 μ M) treatment (Fig. 1a). Quantification of the data demonstrated that CoCl₂ significantly increased EAAC1 expression (CON, 1.04 \pm 0.14; 50 μ M CoCl₂, 1.13 \pm 0.29; 100 μ M CoCl₂, 1.71 \pm 0.12; 150 μ M CoCl₂, 1.88 \pm 0.18; 200 μ M CoCl₂, 2.58 \pm 0.56; 300 μ M CoCl₂, 3.58 \pm 0.56; 500 μ M CoCl₂, 5.87 \pm 0.34; *n* = 8; ****P* < 0.001; Fig. 1b). CoCl₂ treatment significantly increased EAAC1 protein expression at each subsequent time point (0, 1, 3, 6, 12, 24, 36, and 48 h). EAAC1 protein expression was significantly increased after exposure to 100 μ M CoCl₂ for >24 h compared with that of the controls (*n* = 6; **P* < 0.05, ****P* < 0.001; Fig. 1c and d). Next, we investigated whether EAAC1 overexpression affects the cellular cytotoxicity induced by CoCl₂. Treatment with 100 μ M CoCl₂ for 36 h significantly induced cytotoxicity in both the Mock and EAAC1 transfection groups (Mock: CON, 25.85 \pm 1.12; CoCl₂, 57.43 \pm 1.02; *n* = 4; ****P* < 0.001, EAAC1-myc: CON, 23.03 \pm 1.02; CoCl₂, 48.88 \pm 1.64; *n* = 4; ###*P* < 0.001; Fig. 1e). EAAC1 transfection reduced CoCl₂-induced LDH release in SH-SY5Y

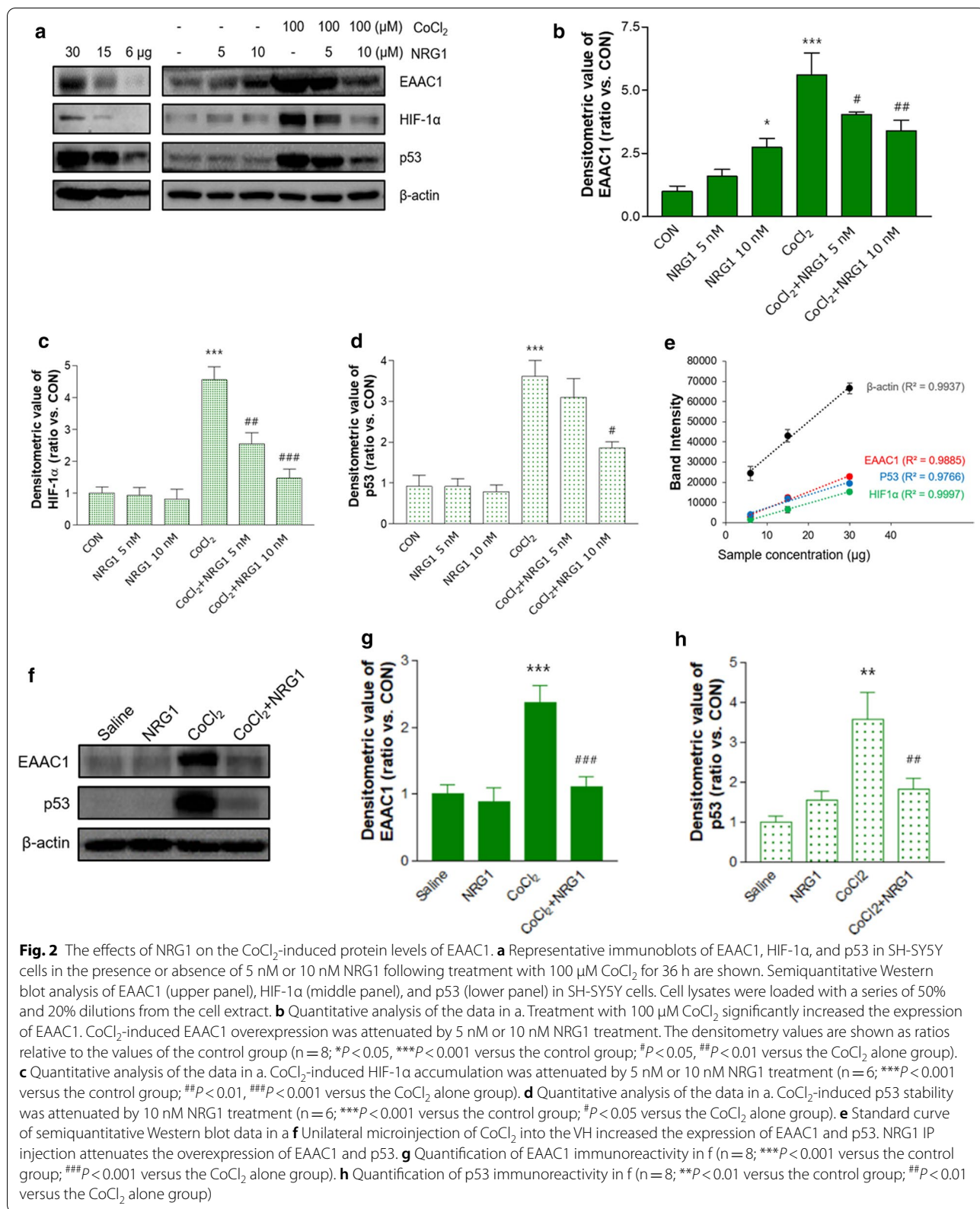
cells (Mock: 57.43 \pm 1.02; EAAC1-myc 48.88 \pm 1.64; *n* = 4; ++*P* < 0.01, Fig. 1e).

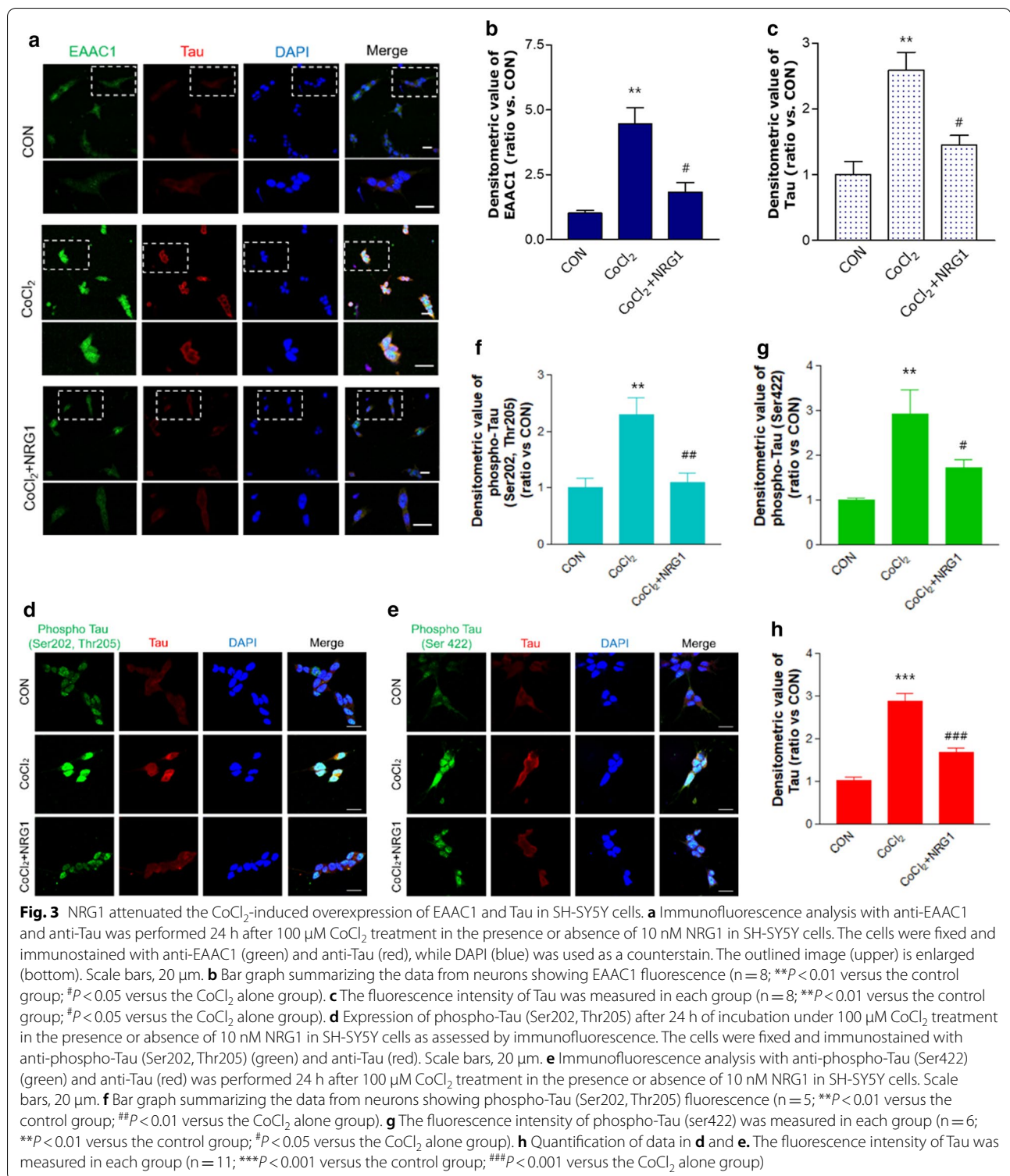
We next analysed the expression of EAAC1 induced by CoCl₂ microinjections in the VH in mice. EAAC1 protein levels were remarkably increased in the VH of the CoCl₂ group (saline, 1.00 \pm 0.15; CoCl₂, 2.06 \pm 0.09; *t*(14) = 5.680 in the DG; ****P* < 0.001; saline, 1.00 \pm 0.07; CoCl₂, 1.40 \pm 0.05; *t*(14) = 4.266 in the CA1; ****P* < 0.001; saline, 1.00 \pm 0.23; CoCl₂, 1.52 \pm 0.10; *t*(14) = 5.158 in the CA3; **P* < 0.05; Fig. 1f–l).

NRG1 alleviated CoCl₂-induced upregulation of EAAC1 in SH-SY5Y cells and the hippocampus of mice

To determine whether NRG1 affected the CoCl₂-induced increase in EAAC1 expression, we pretreated cells with NRG1 (5 nM or 10 nM) for 15 min before CoCl₂ administration. Treatment with 100 μ M CoCl₂ for 36 h significantly upregulated EAAC1 expression (CON, 0.99 \pm 0.21; CoCl₂, 5.61 \pm 0.87; *n* = 8; ****P* < 0.001; Fig. 2a and b). Treatment with 5 nM or 10 nM NRG attenuated the increase in EAAC1 expression induced by 100 μ M CoCl₂ (CoCl₂, 5.61 \pm 0.87; CoCl₂ + 5 nM NRG1, 4.05 \pm 0.09; CoCl₂ + 10 nM NRG1, 3.39 \pm 0.43; *n* = 8; #*P* < 0.05, ##*P* < 0.01; Fig. 2a and b). As shown in Fig. 2a, c and d, treatment with 100 μ M CoCl₂ for 36 h significantly upregulated HIF-1 α (CON, 1.01 \pm 0.19; 100 μ M CoCl₂, 4.56 \pm 0.41; *n* = 6; ****P* < 0.001) and p53 (CON, 0.92 \pm 0.27; 100 μ M CoCl₂, 3.62 \pm 0.38; *n* = 6; ****P* < 0.001) expression. Pretreatment with NRG1 for 36 h attenuated this increase in HIF-1 α accumulation induced by 100 μ M CoCl₂ (CoCl₂, 4.56 \pm 0.41; CoCl₂ + 5 nM NRG1, 2.55 \pm 0.35; CoCl₂ + 10 nM NRG1, 1.47 \pm 0.28; *n* = 6; #*P* < 0.01, ###*P* < 0.001; Fig. 2c). Moreover, pretreatment with 5 nM or 10 nM NRG1 for 36 h attenuated the increase in p53 stabilization induced by 100 μ M CoCl₂ (CoCl₂, 3.62 \pm 0.38; CoCl₂ + 5 nM NRG1, 3.10 \pm 0.46; CoCl₂ + 10 nM NRG1, 1.85 \pm 0.15; *n* = 6; #*P* < 0.05; Fig. 2d). In addition, we confirmed these results based on a semiquantitative Western blot of EAAC1, HIF-1 α , and p53 expression in SH-SY5Y cells (Fig. 2a and e). These results are consistent with those of our previous studies demonstrating the effects of NRG1 on HIF-1 α or p53 [24]. To verify these results in vivo, we treated mice brains with vehicle or NRG1 (50 ng/kg, IP) for 3 days before CoCl₂ microinjection into the VH. After CoCl₂ microinjection, the mice continued receiving NRG1 for 2 days, and then the mice were sacrificed (Fig. 2f). Consistent with the in vitro results, NRG1 dramatically prevented the increase in EAAC1 (CON, 1.00 \pm 0.14; NRG1, 0.89 \pm 0.20; CoCl₂, 2.38 \pm 0.23; CoCl₂ + NRG1, 1.11 \pm 0.14; *n* = 5; ****P* < 0.001, ###*P* < 0.001; Fig. 2g and h)







and p53 expression (CON, 1.00 ± 0.13 ; NRG1, 1.57 ± 0.19 ; CoCl_2 , 3.59 ± 0.60 ; $\text{CoCl}_2 + \text{NRG1}$, 1.82 ± 0.25 ; $n=5$; $**P<0.01$, $\#P<0.01$; Fig. 2g and i) induced by CoCl_2 microinjection in the hippocampus of the mouse brain.

NRG1 inhibited CoCl_2 -induced increases in EAAC1, Tau, and phospho-Tau immunoreactivity

We examined the immunoreactivity of EAAC1 in SH-SY5Y cells using immunofluorescence staining. To

measure the effects of NRG1 on SH-SY5Y cells, cells were pretreated for 15 min with 10 nM NRG1 and then treated with 100 μ M CoCl₂ (Fig. 3a). Treatment with 100 μ M CoCl₂ for 24 h significantly upregulated EAAC1 expression in comparison to that of the control group (CON, 1.02 \pm 0.10; 100 μ M CoCl₂, 4.45 \pm 0.64; n = 8; ***P* < 0.01; Fig. 3b). We also confirmed that the pretreatment of SH-SY5Y cells with 10 nM NRG1 for 24 h significantly attenuated EAAC1 overexpression (CoCl₂, 4.45 \pm 0.64; CoCl₂ + 10 nM NRG1, 1.83 \pm 0.37; n = 8; #*P* < 0.05; Fig. 3b) compared with that of the control group. Interestingly, treatment with 100 μ M CoCl₂ for 24 h markedly increased the accumulation of Tau in comparison with that of the control group (CON, 1.00 \pm 0.20; CoCl₂, 2.58 \pm 0.27; n = 8; ***P* < 0.01; Fig. 3c). Pretreatment with 10 nM NRG1 attenuated the CoCl₂-induced increase in Tau expression (CoCl₂, 2.58 \pm 0.27; CoCl₂ + NRG1, 1.45 \pm 0.15; n = 8; #*P* < 0.05; Fig. 3c). Furthermore, phospho-Tau (Ser202, Thr205) levels were increased in CoCl₂-treated cells (CON, 1.00 \pm 0.15; 100 μ M CoCl₂, 2.29 \pm 0.28; n = 8; ***P* < 0.01; Fig. 3d and f), and pretreatment with 10 nM NRG1 attenuated the CoCl₂-induced increase in phospho-Tau (Ser202, Thr205) expression (CoCl₂, 2.29 \pm 0.28; CoCl₂ + NRG1, 1.10 \pm 0.15; n = 5; ##*P* < 0.01; Fig. 3d and f). In addition, phospho-Tau (Ser422) levels were increased in CoCl₂-treated cells (CON, 1.00 \pm 0.04; 100 μ M CoCl₂, 2.92 \pm 0.49; n = 6; ***P* < 0.01; Fig. 3e and g), and pretreatment with 10 nM NRG1 prevented the CoCl₂-induced increase in phospho-Tau (Ser422) expression (CoCl₂, 2.92 \pm 0.49; CoCl₂ + NRG1, 1.72 \pm 0.17; n = 6; #*P* < 0.05; Fig. 3e and g). We confirmed that 10 nM NRG1 pretreatment attenuated the CoCl₂-induced increase in Tau expression (CON, 1.00 \pm 0.13; CoCl₂, 2.78 \pm 0.28; CoCl₂ + NRG1, 1.69 \pm 0.08; n = 11; ****P* < 0.001, ###*P* < 0.001; Fig. 3d, e, and h).

NRG1 rescued CoCl₂-induced ROS generation and the reduction in antioxidant enzymes in SH-SY5Y cells

We tested the protective effect of NRG1 against CoCl₂-induced ROS generation. We found that treatment with 100 μ M CoCl₂ for 24 h significantly increased ROS levels (CON, 1.13 \pm 0.20; CoCl₂, 4.46 \pm 0.44; n = 6; ****P* < 0.001; Fig. 4a and b) compared with the levels in the control group. However, pretreatment with 5 nM or 10 nM NRG1 significantly attenuated CoCl₂-induced ROS generation (CoCl₂, 4.46 \pm 0.44; CoCl₂ + 5 nM NRG1, 2.70 \pm 0.37; CoCl₂ + 10 nM NRG1, 1.67 \pm 0.16; n = 6; #*P* < 0.05, ##*P* < 0.01; Fig. 4a and b). To determine whether NRG1 affects the antioxidant defense system, we analyzed the activity of the antioxidant enzymes GPx and SOD. Treatment with 100 μ M CoCl₂ significantly reduced the activity of GPx (CON, 32.37 \pm 1.63; CoCl₂,

19.31 \pm 1.77; n = 6; ***P* < 0.01; Fig. 4c) compared with that of the control group. Pretreatment with 5 nM or 10 nM NRG1 for 36 h attenuated the CoCl₂-induced reduction in GPx activity (CoCl₂, 19.31 \pm 1.77; CoCl₂ + 5 nM NRG1, 34.38 \pm 1.94; CoCl₂ + 10 nM NRG1, 30.46 \pm 1.99; n = 6; ###*P* < 0.001; Fig. 4c). Moreover, after the cells were exposed to 100 μ M CoCl₂ in the presence or absence of NRG1 for 36 h, SOD activity was measured. We also demonstrated that after the cells were exposed to CoCl₂ for 36 h, there were distinct decreases in SOD activity (CON, 121.78 \pm 2.88; CoCl₂, 98.91 \pm 5.02; n = 8; ****P* < 0.001; Fig. 4d). Moreover, pretreatment of cells with 5 nM or 10 nM NRG1 attenuated the CoCl₂-induced decrease in SOD activity (CoCl₂, 98.91 \pm 5.02; CoCl₂ + 5 nM NRG1, 116.74 \pm 2.51; CoCl₂ + 10 nM NRG1, 114.189 \pm 3.76; n = 8; #*P* < 0.05, ##*P* < 0.01; Fig. 4d).

NRG1 treatment reduced superoxide generation induced by microinjection of CoCl₂ into the VH of mice.

To further demonstrate that NRG1 protects against ROS generation in vivo, we determined the amount of hippocampal superoxide content as a major ROS form by DHE staining. We investigated the generation of superoxide in the DG (top panels), CA1 (middle panels), and CA3 (bottom panels) regions of the VH by microinjection of CoCl₂ (DG: saline, 1.00 \pm 0.13; CoCl₂, 2.36 \pm 0.27; n = 8; **P* < 0.05; CA1: saline, 1.00 \pm 0.08; CoCl₂, 2.36 \pm 0.14; n = 8; ****P* < 0.001; CA3: saline, 1.00 \pm 0.15; CoCl₂, 2.13 \pm 0.07; n = 8; ****P* < 0.001; Fig. 5a-d). NRG1 injection in mice of micro-injected CoCl₂ alleviated the increase in superoxide generation in the DG, CA1, and CA3 (DG: CoCl₂, 2.36 \pm 0.27; CoCl₂ + NRG1, 0.90 \pm 0.09; n = 8; ##*P* < 0.01; CA1: CoCl₂, 2.36 \pm 0.14; CoCl₂ + NRG1, 1.04 \pm 0.05; n = 8; ###*P* < 0.001; CA3: CoCl₂, 2.13 \pm 0.07; CoCl₂ + NRG1, 1.01 \pm 0.11; n = 8; ###*P* < 0.001; Fig. 5a-d).

NRG1 rescued CoCl₂-induced apoptosis and cell death

We examined whether NRG1 affects CoCl₂-induced apoptosis in SH-SY5Y cells. To detect apoptotic nuclei in SH-SY5Y cells, we used TUNEL staining. Treatment with 100 μ M CoCl₂ significantly increased the proportion of apoptotic nuclei (CON, 2.00 \pm 0.58; CoCl₂, 21.33 \pm 2.03; n = 6; ****P* < 0.001; Fig. 6a and b) compared with that of the control group. Pretreatment with 10 nM NRG1 for 24 h reduced the number of CoCl₂-induced TUNEL-positive cells (CoCl₂, 21.33 \pm 2.03; CoCl₂ + 10 nM NRG1, 6.33 \pm 2.03; n = 6; ##*P* < 0.01, Fig. 6a and b).

Next, we examined CoCl₂-induced cytotoxicity in SH-SY5Y cells. The cells were incubated with 10 nM NRG1 and then exposed to 100 μ M CoCl₂ for 36 h (CON, 10.48 \pm 2.10; CoCl₂, 31.97 \pm 3.21; CoCl₂ + 10 nM NRG1, 16.18 \pm 2.05; n = 6; ***P* < 0.01, #*P* < 0.05; Fig. 6c).

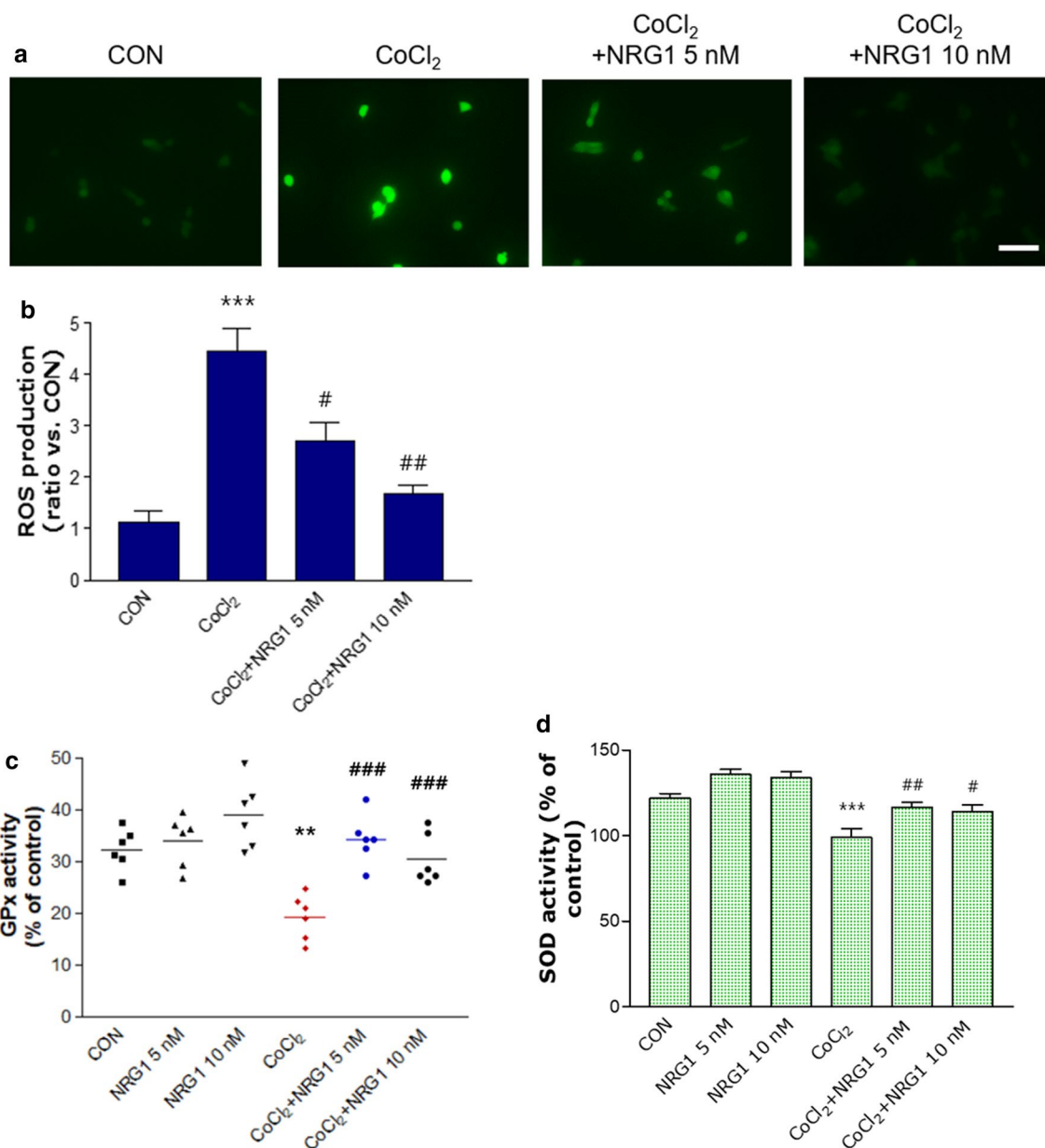


Fig. 4 NRG1 reduced the increase in ROS and decreased oxidative stress-related enzyme activity induced by CoCl₂. **a** After 24 h, intracellular ROS levels were measured by fluorescence microscopy using DCFH-DA dye that was administered to 100 μM CoCl₂-treated SH-SY5Y cells that had been pretreated with NRG1 (5 or 10 nM) for 15 min. **b** Bar graph summarizing the data in **a** (n=6; ***P<0.001 versus the control group; #P<0.05, ##P<0.01 versus the CoCl₂ alone group). **c** SH-SY5Y cells were treated with 100 μM CoCl₂ alone or with PBS or NRG1 (5 nM or 10 nM) for 36 h. GPx activity was measured using a GPx assay kit (Cayman Chemical Company, MI, USA) (n=6; **P<0.01 versus the control group; ###P<0.001 versus the CoCl₂ alone group). **d** After the SH-SY5Y cells were exposed to 100 μM CoCl₂ in the presence or absence of NRG1 (5 nM or 10 nM) for 36 h, SOD activity was evaluated by measuring the inhibition of the reduction of tetrazolium salt by xanthine-xanthine oxidase according to the manufacturer's instructions (Cayman Chemical Company, MI, USA). The SOD assay measured all three types of SOD (FeSOD, Cu/An, and Mn) (n=8; ***P<0.001 versus the control group; #P<0.05, ##P<0.01 versus the CoCl₂ alone group)

Effects of NRG1 on CoCl₂-induced changes in apoptotic or antiapoptotic proteins

We next investigated whether caspase-3 cleavage is increased by CoCl₂. SH-SY5Y cells were treated with

100 μM CoCl₂ for 24 h before fixation and immunofluorescence detection of cleaved caspase-3. We found that CoCl₂ increased the cleavage of caspase-3, and quantitative analysis showed that the number of cleaved

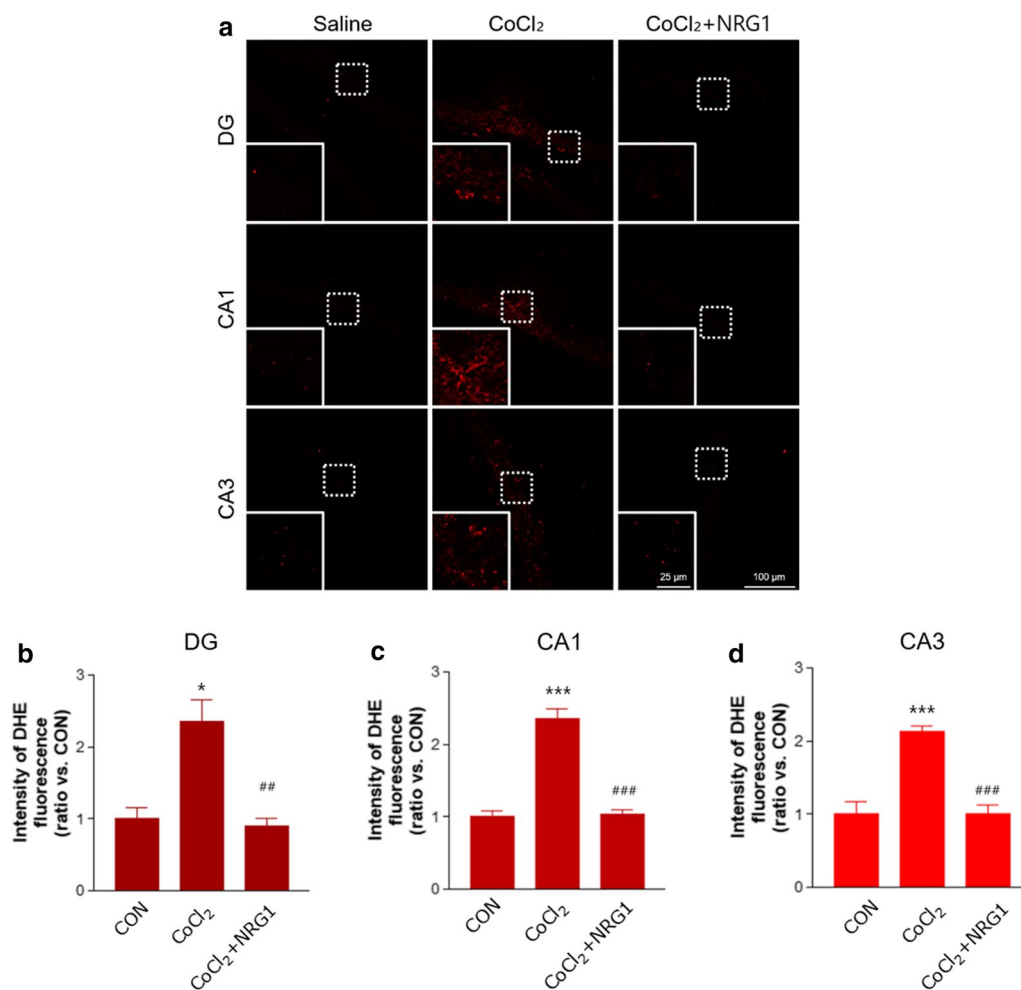


Fig. 5 NRG1 treatment reduced superoxide generation induced by microinjection of CoCl₂ into the VH of mice. **a** Photomicrographs reveal the generation of superoxide in the DG (top panels), CA1 (middle panels), and CA3 (bottom panels) regions of the VH in the Saline, CoCl₂, and CoCl₂ + NRG1 groups. Increased superoxide generation of VH induced by microinjection with CoCl₂ (1 μl-25 mM) was measured by fluorescence microscopy using the DHE dye. The mice were treated with NRG1 (50 ng/kg) for 5 days. Scale bar, 100 μm; inset, enlarged areas. Scale bar, 25 μm. **b** Bar graph summarizing the data in a (DG) (n = 8; *P < 0.05 versus the saline group; ##P < 0.01 versus the CoCl₂ alone group). **c** Bar graph summarizing the data in a (CA1) (n = 8; ***P < 0.001 versus the saline group; ###P < 0.001 versus the CoCl₂ alone group). **d** Bar graph summarizing the data in a (CA2) (n = 8; ***P < 0.001 versus the saline group; ###P < 0.001 versus the CoCl₂ alone group)

caspase-3-positive cells was increased (CON, 1.00 ± 0.51 ; CoCl₂, 3.40 ± 0.34 ; n = 6; **P < 0.01; Fig. 7a and b). Furthermore, pretreatment with 10 nM NRG1 for 24 h rescued the CoCl₂-induced increase in the number of cleaved caspase-3-positive cells (CoCl₂, 3.40 ± 0.34 ; CoCl₂ + 10 nM NRG1, 1.93 ± 0.35 ; n = 6; #P < 0.05, Fig. 7a and b). To determine whether NRG1 regulates CoCl₂-induced caspase-3 cleavage, we performed western blotting. We observed that the level of cleaved caspase-3 (17 and 19 kD) was significantly increased after CoCl₂ treatment (CON, 1.28 ± 0.16 ; CoCl₂, 2.56 ± 0.29 ; n = 6; **P < 0.01; Fig. 7c and d). NRG1 attenuated the CoCl₂-induced increase in cleaved caspase-3

(CoCl₂, 2.56 ± 0.29 ; CoCl₂ + 5 nM NRG1, 1.52 ± 0.17 ; CoCl₂ + 10 nM NRG1, 1.13 ± 0.10 ; n = 6; #P < 0.05, ##P < 0.01; Fig. 7c and d). Furthermore, the expression of Bcl-X_L (an antiapoptotic protein) was decreased in CoCl₂-induced cells (CON, 1.02 ± 0.14 ; CoCl₂, 0.4 ± 0.08 ; n = 6; *P < 0.05; Fig. 7c and e). NRG1 protected against the CoCl₂-induced reduction in Bcl-xL protein expression (CoCl₂, 0.4 ± 0.08 ; CoCl₂ + 5 nM NRG1, 0.66 ± 0.05 ; CoCl₂ + 10 nM NRG1, 1.01 ± 0.11 ; n = 6; #P < 0.05; Fig. 7c and e). These results suggest that NRG1 may have a protective role under hypoxic conditions by regulating apoptosis. In addition, we confirmed the effect of NRG1 on the upregulation of EAAC1 by transient transfection in

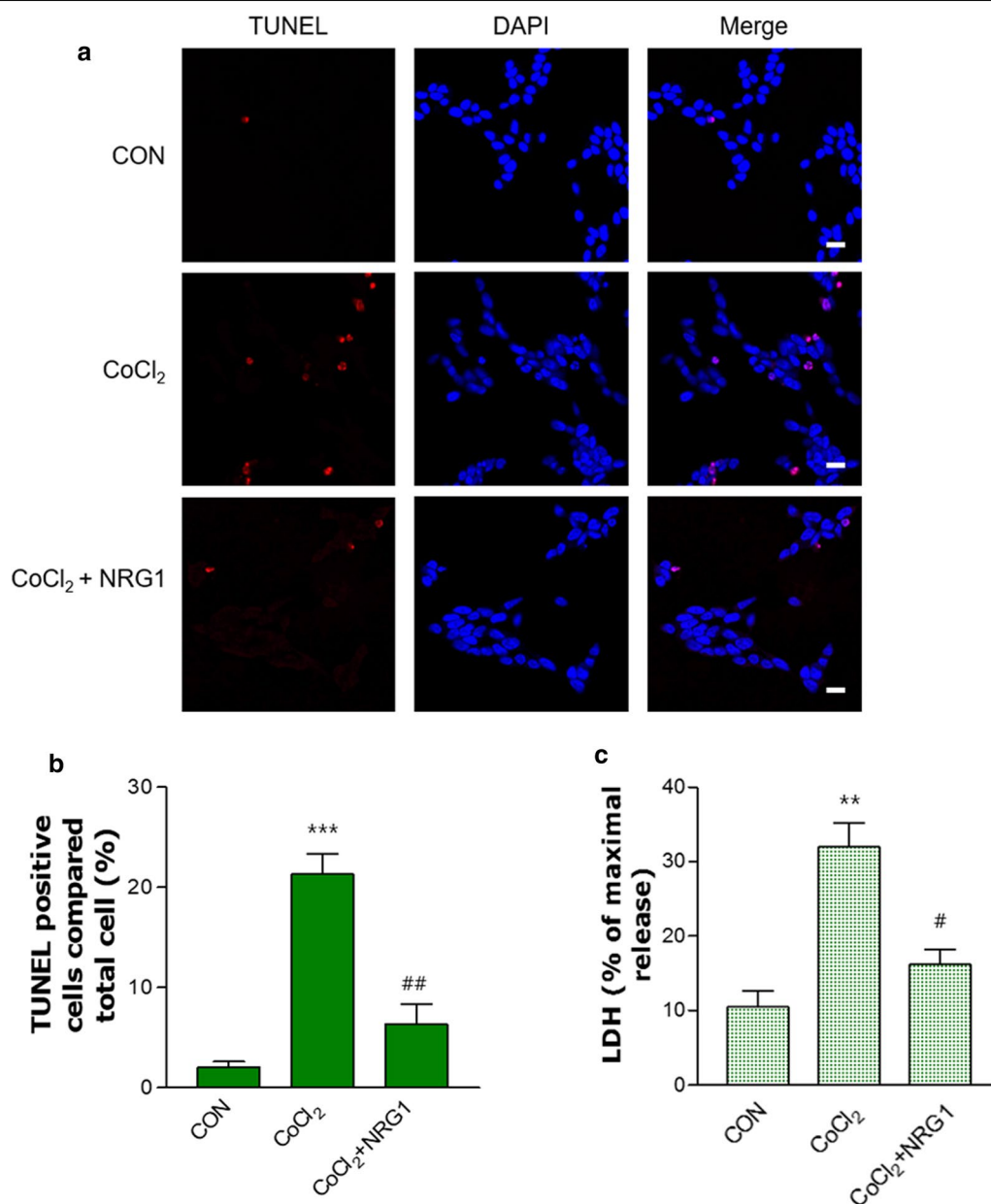


Fig. 6 NRG1 attenuated CoCl₂-induced apoptosis and cell death in SH-SY5Y cells. **a** TUNEL staining (red) showing the amount of apoptosis that occurred in cells treated with 100 μM CoCl₂ and either PBS or 10 nM NRG1 for 24 h. DAPI (blue) was used as a counterstain. Scale bars, 20 μm. **b** Apoptotic cells are expressed as the percentage of TUNEL-positive cells relative to the number of DAPI-stained cells (n = 6; ***P < 0.001 versus the control group; **P < 0.01 versus the CoCl₂ alone group). **c** NRG1 (10 nM) attenuated cell death induced by 100 μM CoCl₂ in SH-SY5Y cells. After 36 h, the degree of cell death was measured by LDH activity in the medium (n = 6; **P < 0.01 versus the control group; #P < 0.05 versus the CoCl₂ alone group)

CoCl₂-induced apoptosis. EAAC1 transfection reduced CoCl₂-induced caspase-3 cleavage (Mock: 2.78 ± 0.13; EAAC1-myc: 2.13 ± 0.14; n = 6; +++P < 0.01; Fig. 7f and g). NRG1 attenuated CoCl₂-induced increases in cleaved caspase-3 in both Mock (CON, 1.00 ± 0.08; CoCl₂, 2.78 ± 0.13; CoCl₂ + 5 nM NRG1, 2.18 ± 0.11;

n = 6; ***P < 0.001, **P < 0.01; Fig. 7f and g) and EAAC1-myc (CON, 1.14 ± 0.09; CoCl₂, 2.13 ± 0.14; CoCl₂ + 5 nM NRG1, 1.28 ± 0.20; n = 6; ***P < 0.001, ###P < 0.001; Fig. 7f and g).

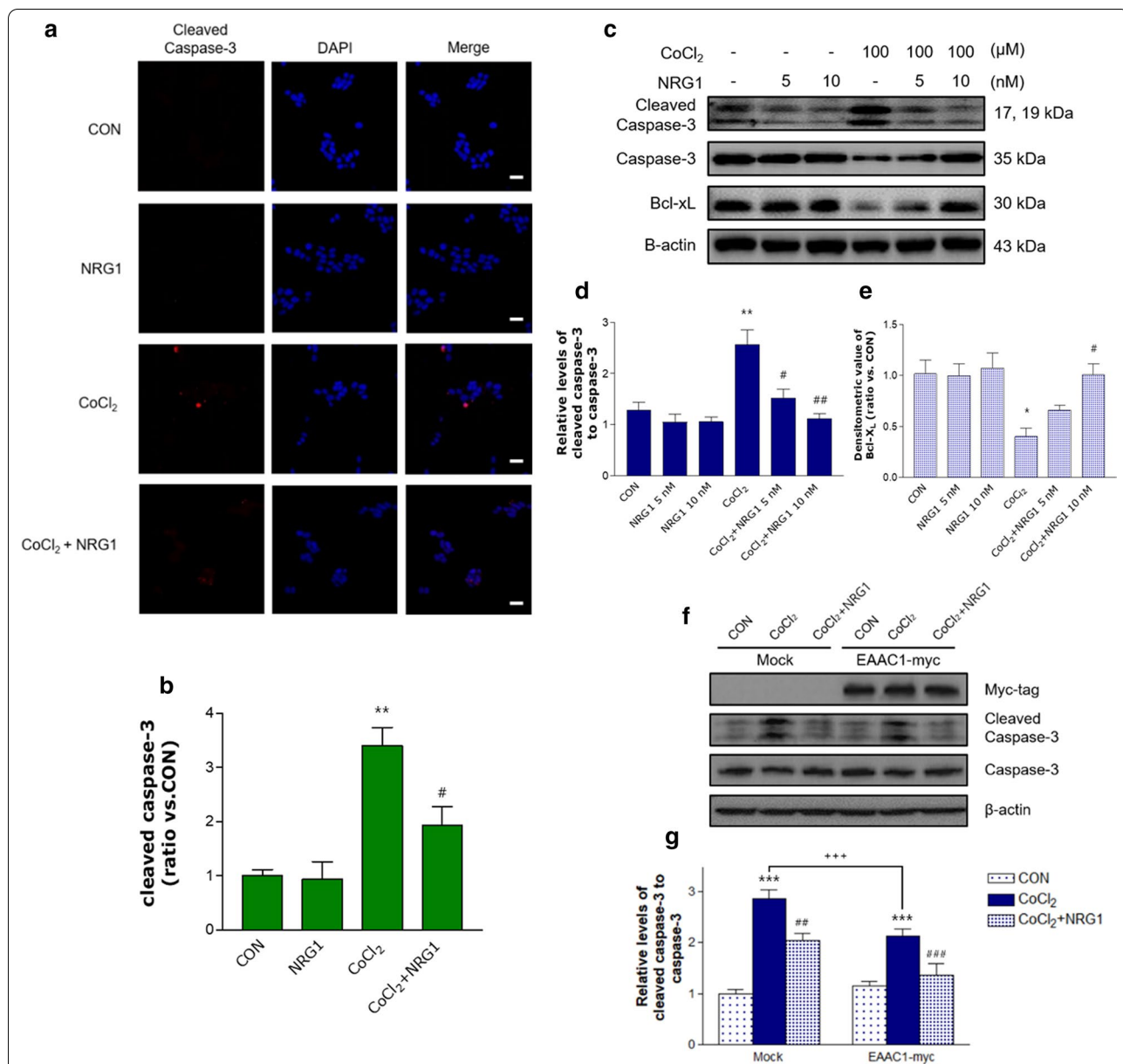


Fig. 7 The effects of NRG1 on the CoCl₂-induced protein levels of cleaved caspase-3 and Bcl-X_L. **a** Representative immunofluorescence image of cells after treatment with 100 μM CoCl₂ in the presence or absence of 10 nM NRG1 for 24 h. Cells were fixed and immunostained with anti-cleaved caspase-3 (red) and counterstained with DAPI (blue). Cleaved caspase-3 staining was significantly higher in CoCl₂-only treated cells than in control cells. NRG1 protected against CoCl₂-induced expression of cleaved caspase-3. **b** The ratio of cleaved caspase-3-positive cells to the total number of cells (n = 6; *******P* < 0.01 versus the control group; **#***P* < 0.05 versus the CoCl₂ alone group). Scale bars, 20 μm. **c** Protein expression of Bcl-X_L, cleaved caspase-3, caspase-3 and β-actin was analyzed by western blotting. Representative immunoblots showing SH-SY5Y cells treated with 100 μM CoCl₂ and either PBS or NRG1 (5 nM or 10 nM) for 36 h. **d** Quantitative analysis of the data in a. Treatment with CoCl₂ significantly increased the expression of cleaved caspase-3. NRG1 attenuated the increase in cleaved caspase-3 expression, as shown by the densitometric values (n = 6; *******P* < 0.01 versus the control group; **#***P* < 0.05, **##***P* < 0.01 versus the CoCl₂ alone group). **e** Quantitative analysis of the data in a. Treatment with CoCl₂ significantly decreased the expression of Bcl-X_L in SH-SY5Y cells. NRG1 inhibited the reduction in Bcl-X_L expression, as shown by the densitometric values (n = 6; ******P* < 0.05 versus the control group; **#***P* < 0.05 versus the CoCl₂ alone group). **f** Protein expression of myc-tag, cleaved caspase-3, caspase-3, and β-actin was analysed after EAAC1-myc transfection. **g** Representative immunoblots of SH-SY5Y cells treated with 100 μM CoCl₂ and either PBS or NRG1 (5 nM) for 36 h. Quantitative analysis of the data in f (Mock: n = 6; ********P* < 0.001 versus the control group; **##***P* < 0.01 versus the CoCl₂ alone group; EAAC1-myc: n = 6; ********P* < 0.001 versus the control group; **###***P* < 0.001 versus the CoCl₂ alone group). EAAC1 transfection reduced CoCl₂-induced cleaved caspase-3 (n = 6; **+++***P* < 0.001)

Discussion

In the present study, we assessed the effects and mechanisms of NRG1 on CoCl₂-induced oxidative stress in SH-SY5Y cells and the hippocampus of mice. First, we demonstrated that CoCl₂ dramatically increased EAAC1 protein expression in SH-SY5Y cells. We also confirmed the increased EAAC1 expression by CoCl₂ microinjection in the VH in mice. EAAT1 and EAAT2 are mainly expressed in glial cells [27–29], whereas EAAT3 is exclusively expressed in neurons [30–33]. The EAAC1 protein is abundantly expressed in the hippocampus, cerebellum, and midbrain areas [31]. In general, EAAC1 activity is considered to be the main mechanism responsible for glutamatergic transmission [2], and EAAC1 also transports cysteine into neurons [34, 35]. Modulation of EAAC1 activity correlates with neuronal GSH levels [7] and the rate-limiting substrate for neuronal synthesis of GSH [36].

EAAC1 may be the major contributor to GSH synthesis [5] in neurons. Interestingly, Rossi et al. reported that glutamate release is largely mediated by reversed activity of the neuronal glutamate transporter in severe brain ischemia. The glutamate transporter plays a key role in generating anoxic depolarization in hippocampal neurons [37]. These results suggest that the abnormal activity abolished information processing in the CNS within minutes of ischemia EAAC1-deficient mice showed that the delayed anoxic depolarization [38], overexpression of EAAC1 could contribute to the reversed activity in neurons. *SLC1A1* encodes EAAC1, a *SLC1A1* polymorphism highly replicated in obsessive–compulsive disorder studies that is associated with increased transcript levels in human brain tissue [39, 40]. Mice with EAAC1 overexpression displayed increased anxiety-like and repetitive behaviours and synaptic alterations [41]. Even if our data demonstrate that the transient transfection of EAAC1-myc reduced CoCl₂-induced cell death and oxidative stress in SH-SY5Y cells, the abnormal overexpression of EAAC1 by chronic hypoxic stress might alter synaptic function and neuronal circuits in animal models.

Hypoxic conditions have been extensively studied for their potential to regulate glutamate transporters, as this putative regulation could have important consequences for brain pathologies. A previous study reported that chronic hypoxia upregulates EAAC1 expression in PC12 cells [42]. CoCl₂ was reported to be a widely used hypoxia mimetic in a large variety of cells and is known to both inhibit prolyl hydroxylases, leading to HIF-1 α stabilization, and induce ROS formation under normoxic conditions [43, 44]. In addition, direct CoCl₂ brain microinjection provides a valuable animal model to develop focal ischemia in selected brain regions to study their

functional consequences and potential pharmacological therapies.

Furthermore, we examined the effect of NRG1 on CoCl₂-induced EAAC1 and hypoxia-related protein. Several lines of evidence collectively suggest that NRG1 plays a neuroprotective role in the brain against neurotoxic substances related to apoptosis and oxidative damage in neurons [45–48]. In this study, we showed that NRG1 could prevent CoCl₂-induced upregulation of EAAC1 levels in SH-SY5Y cells and the hippocampus of brain. We also confirmed that NRG1 could attenuate the CoCl₂-induced accumulation of HIF-1 α and p53 [24]. Immunofluorescence analysis also showed that NRG1 significantly inhibited CoCl₂-induced overexpression of EAAC1 in SH-SY5Y cells. Tau protein is a soluble microtubule-associated protein that is abundant in neurons and plays a role in neurite outgrowth and axonal transport [49, 50]. Additionally, the level of Tau and phospho-Tau increased in cells after CoCl₂ treatment, suggesting that hypoxia or oxidative stress can lead to alterations in cell structure. Previously, there was a report showing that hypoxia promoted the phosphorylation and total expression of tau protein [42, 51]. Additional evidence suggests that hypoxic and ischaemic brain damage in humans and animals may contribute to tau protein dysfunction, which is proposed as a risk factor for developing Alzheimer's disease (AD) [52]. The model generated using the hypoxia-mimicking agent CoCl₂ excluded environmental and vascular factors; thus, it could be useful to investigate the correlation between cellular hypoxia and AD. Moreover, we found that NRG1 prevented the CoCl₂-induced upregulation of EAAC1, Tau and phospho-Tau.

Next, we examined whether NRG1 protects against CoCl₂-induced ROS generation. Numerous studies have suggested that hypoxia induces increased production of ROS in the brain [53–55]. When we treated the cells with CoCl₂, ROS levels were increased. According to our results, NRG1 attenuated the CoCl₂-induced generation of ROS in SH-SY5Y cells. There is a balance between the generation of ROS and their clearance by antioxidant networks, mainly by GPx, SOD, and catalase under physiological conditions [56, 57]. In the present study, CoCl₂ reduced the activity of GPx and SOD in SH-SY5Y cells. We found that NRG1 had a protective effect on the CoCl₂-induced reduction in GPx and SOD enzymatic activity. Furthermore, we confirmed that NRG1 reduced superoxide generation induced by microinjection of CoCl₂ into the VH of brain. ROS is a powerful initiator of apoptosis, which also contributes to hypoxia-mediated neuronal cell death [58]. We also found that NRG1 significantly reduced CoCl₂-induced apoptosis and cell death in SH-SY5Y cells.

In the intrinsic pathway, ROS induce mitochondria-dependent apoptosis. This process can be modulated by the release of cytochrome c and the downstream activation of caspases. We next focused on whether NRG1 could protect SH-SY5Y cells against the activation of caspase-3 after CoCl₂ treatment. Our results verified that NRG1 significantly reduced the expression of cleaved caspase-3, which may have prevented hypoxia-induced apoptosis and cell death in SH-SY5Y cells. Immunoblot analysis also confirmed the effect of NRG1 on the CoCl₂-induced activation of caspase-3. Bcl-2 family members act as critical regulators of the intrinsic apoptotic pathway. The antiapoptotic Bcl-2 family protein Bcl-X_L predominantly localizes to the outer mitochondrial membrane, whereas other members indirectly interact with mitochondria [59]. We further confirmed that NRG1 inhibited the CoCl₂-induced reduction in Bcl-xL expression. Taken together, our data suggest that NRG1 protects against CoCl₂-induced overexpression of EAAC1.

Pretreatment with NRG1 could activate these cellular defense mechanisms to mimic hypoxic preconditioning. NRG1 exerts its biological effects by activating a family of ErbB tyrosine kinase receptors. NRG1 can trigger signaling pathways such as Raf-MEK-ERK and PI3K-Akt-S6K. Further study is needed to clarify the underlying pathway associated with NRG1 in these effects.

Conclusion

Our study suggests that CoCl₂ significantly increases EAAC1 expression in SH-SY5Y cells and the hippocampus of mice. NRG1 attenuates the CoCl₂-induced overexpression of EAAC1 and reduces CoCl₂-induced oxidative stress and apoptotic signaling. NRG1 potentially plays a protective role in hypoxia through the inhibition of oxidative stress and maintains normal EAAC1 expression levels.

These results may show a new path toward understanding the pathogenesis and treatment of hypoxia and oxidative stress-related neurological diseases.

Abbreviations

EAAC1: Excitatory amino acid carrier 1 (also referred to as EAAT3); EAAT: Excitatory amino acid transporter; CNS: Central nervous system; GSH: Glutathione; HIF-1: Hypoxia inducible factor-1; OGD: Oxygen–glucose deprivation; NRG1: Neuregulin 1; CoCl₂: Cobalt chloride; ROS: Reactive oxygen species; LDH: Lactate Dehydrogenase; TUNEL: Terminal deoxynucleotidyl transferase dUTP nick end labeling; GPx: Glutathione peroxidase; SOD: Superoxide dismutase; DHE: Dihydroethidium; VH: Ventral hippocampus.

Authors' contributions

HBK, JYY performed the experiments. HSK and JHL performed the data analysis. HBK, TKB, and RSW designed the study and wrote the manuscript. All authors critically reviewed the content. All authors read and approved the final manuscript.

Funding

This work was supported by the National Research Foundation of Korea (NRF) and funded by the Ministry of Education, Science and Technology (NRF-2019R1H1A2079060 awarded to RSW, NRF-2020R1A2C1011839 awarded to HSK and 2017R1D1A1B03028729 awarded to JHL).

Availability of data and materials

Please contact author for data requests.

Ethics approval and consent to participate

Not applicable.

Consent for publication

Not applicable.

Competing interests

The authors declare no competing financial interests.

Author details

¹ Department of Anatomy and Neuroscience, College of Medicine, Eulji University, 143-5Jung-Gu, Yongdu-Dong, Daejeon 301-746, Republic of Korea. ² Department of Emergency Medical Technology, Daejeon University, Daejeon 34520, Republic of Korea. ³ Department of Physiology, College of Medicine, Eulji University, Daejeon 301-746, Republic of Korea. ⁴ Department of Pharmacology, College of Medicine, Seoul National University, Seoul 110-799, Korea. ⁵ Seoul National University College of Medicine, Bundang Hospital, Sungnam 13620, Republic of Korea.

Received: 9 July 2020 Accepted: 9 October 2020

Published online: 13 November 2020

References

- Aoyama K, Nakaki T. Neuroprotective properties of the excitatory amino acid carrier 1 (EAAC1). *Amino Acids*. 2013;45(1):133–42.
- Bianchi MG, Bardelli D, Chiu M, Bussolati O. Changes in the expression of the glutamate transporter EAAT3/EAAC1 in health and disease. *Cell Mol Life Sci*. 2014;71(11):2001–15.
- Sagara JI, Miura K, Bannai S. Maintenance of neuronal glutathione by glial cells. *J Neurochem*. 1993;61(5):1672–6.
- Kranich O, Hamprecht B, Dringen R. Different preferences in the utilization of amino acids for glutathione synthesis in cultured neurons and astroglial cells derived from rat brain. *Neurosci Lett*. 1996;219(3):211–4.
- De Bundel D, Schallier A, Loyens E, Fernando R, Miyashita H, Van Lieffering J, Vermoesen K, Bannai S, Sato H, Michotte Y, et al. Loss of system x(c)-does not induce oxidative stress but decreases extracellular glutamate in hippocampus and influences spatial working memory and limbic seizure susceptibility. *J Neurosci*. 2011;31(15):5792–803.
- Malik AR, Willnow TE. Excitatory amino acid transporters in physiology and disorders of the central nervous system. *Int J Mol Sci*. 2019;20(22):5671.
- Aoyama K, Watabe M, Nakaki T. Modulation of neuronal glutathione synthesis by EAAC1 and its interacting protein GTRAP3-18. *Amino Acids*. 2012;42(1):163–9.
- Himi T, Ikeda M, Yasuhara T, Nishida M, Morita I. Role of neuronal glutamate transporter in the cysteine uptake and intracellular glutathione levels in cultured cortical neurons. *J Neural Transm (Vienna)*. 2003;110(12):1337–48.
- Movafagh S, Crook S, Vo K. Regulation of hypoxia-inducible factor-1α by reactive oxygen species: new developments in an old debate. *J Cell Biochem*. 2015;116(5):696–703.
- Fleiderovich IA, Gebhardt C, Astman N, Gutnick MJ, Heinemann U. Enhanced spontaneous transmitter release is the earliest consequence of neocortical hypoxia that can explain the disruption of normal circuit function. *J Neurosci*. 2001;21(13):4600–8.
- Roettger V, Lipton P. Mechanism of glutamate release from rat hippocampal slices during in vitro ischemia. *Neuroscience*. 1996;75(3):677–85.

12. Jabaudon D, Scanziani M, Gahwiler BH, Gerber U. Acute decrease in net glutamate uptake during energy deprivation. *Proc Natl Acad Sci USA*. 2000;97(10):5610–5.
13. Szatkowski M, Barbour B, Attwell D. Non-vesicular release of glutamate from glial cells by reversed electrogenic glutamate uptake. *Nature*. 1990;348(6300):443–6.
14. Hsu L, Rockenstein E, Mallory M, Hashimoto M, Masliah E. Altered expression of glutamate transporters under hypoxic conditions in vitro. *J Neurosci Res*. 2001;64(2):193–202.
15. Romera C, Hurtado O, Botella SH, Lizasoain I, Cardenas A, Fernandez-Tome P, Leza JC, Lorenzo P, Moro MA. In vitro ischemic tolerance involves upregulation of glutamate transport partly mediated by the TACE/ADAM17-tumor necrosis factor-alpha pathway. *J Neurosci*. 2004;24(6):1350–7.
16. An SJ, Kang TC, Park SK, Hwang IK, Cho SS, Chung MH, Won MH. Oxidative DNA damage and alteration of glutamate transporter expressions in the hippocampal Ca1 area immediately after ischemic insult. *Mol Cells*. 2002;13(3):476–80.
17. Mei L, Nave KA. Neuregulin-ERBB signaling in the nervous system and neuropsychiatric diseases. *Neuron*. 2014;83(1):27–49.
18. Guo WP, Wang J, Li RX, Peng YW. Neuroprotective effects of neuregulin-1 in rat models of focal cerebral ischemia. *Brain Res*. 2006;1087(1):180–5.
19. Ryu J, Hong BH, Kim YJ, Yang EJ, Choi M, Kim H, Ahn S, Baik TK, Woo RS, Kim HS. Neuregulin-1 attenuates cognitive function impairments in a transgenic mouse model of Alzheimer's disease. *Cell Death Dis*. 2016;7:e2117.
20. Carlsson T, Schindler FR, Hollerhage M, Depboylu C, Arias-Carrion O, Schnurrbusch S, Rosler TW, Wozny W, Schwall GP, Groebe K, et al. Systemic administration of neuregulin-1beta1 protects dopaminergic neurons in a mouse model of Parkinson's disease. *J Neurochem*. 2011;117(6):1066–74.
21. Alizadeh A, Santhosh KT, Kataria H, Gounni AS, Karimi-Abdolrezaee S. Neuregulin-1 elicits a regulatory immune response following traumatic spinal cord injury. *J Neuroinflammation*. 2018;15(1):53.
22. Lan C, Chen X, Zhang Y, Wang W, Wang WE, Liu Y, Cai Y, Ren H, Zheng S, Zhou L, Zeng C. Curcumin prevents strokes in stroke-prone spontaneously hypertensive rats by improving vascular endothelial function. *BMC Cardiovasc Disord*. 2018;18:43.
23. Kim YJ, Yoo JY, Kim OS, Kim HB, Ryu J, Kim HS, Lee JH, Yoo HI, Song DY, Baik TK, et al. Neuregulin 1 regulates amyloid precursor protein cell surface expression and non-amyloidogenic processing. *J Pharmacol Sci*. 2018;137(2):146–53.
24. Yoo SY, Yoo JY, Kim HB, Baik TK, Lee JH, Woo RS. Neuregulin-1 protects neuronal cells against damage due to CoCl_2 -induced hypoxia by suppressing hypoxia-inducible factor-1alpha and P53 in SH-SY5Y Cells. *Int Neurosci J*. 2019;23(Suppl 2):S111–118.
25. Yoo JY, Kim HB, Yoo SY, Yoo HI, Song DY, Baik TK, Lee JH, Woo RS. Neuregulin 1/ErbB4 signaling attenuates neuronal cell damage under oxygen-glucose deprivation in primary hippocampal neurons. *Anat Cell Biol*. 2019;52(4):462–8.
26. Chandel NS, McClintock DS, Feliciano CE, Wood TM, Melendez JA, Rodriguez AM, Schumacker PT. Reactive oxygen species generated at mitochondrial complex III stabilize hypoxia-inducible factor-1alpha during hypoxia: a mechanism of O_2 sensing. *J Biol Chem*. 2000;275(33):25130–8.
27. Chaudhry FA, Lehre KP, van Lookeren CM, Ottersen OP, Danbolt NC, Storm-Mathisen J. Glutamate transporters in glial plasma membranes: highly differentiated localizations revealed by quantitative ultrastructural immunocytochemistry. *Neuron*. 1995;15(3):711–20.
28. Lehre KP, Levy LM, Ottersen OP, Storm-Mathisen J, Danbolt NC. Differential expression of two glial glutamate transporters in the rat brain: quantitative and immunocytochemical observations. *J Neurosci*. 1995;15(3 Pt 1):1835–53.
29. Danbolt NC, Storm-Mathisen J, Kanner BI. An $[\text{Na}^+ + \text{K}^+]$ -coupled L-glutamate transporter purified from rat brain is located in glial cell processes. *Neuroscience*. 1992;51(2):295–310.
30. Holmseth S, Dehnes Y, Huang YH, Follin-Arbelet VV, Grutle NJ, Mylonakou MN, Plachez C, Zhou Y, Furness DN, Bergles DE, et al. The density of EAAC1 (EAAT3) glutamate transporters expressed by neurons in the mammalian CNS. *J Neurosci*. 2012;32(17):6000–13.
31. Rothstein JD, Martin L, Levey AI, Dykes-Hoberg M, Jin L, Wu D, Nash N, Kuncel RW. Localization of neuronal and glial glutamate transporters. *Neuron*. 1994;13(3):713–25.
32. Kanai Y, Bhide PG, DiFiglia M, Hediger MA. Neuronal high-affinity glutamate transport in the rat central nervous system. *NeuroReport*. 1995;6(17):2357–62.
33. Yu HN, Park WK, Nam KH, Song DY, Kim HS, Baik TK, Woo RS. Neuregulin 1 controls glutamate uptake by up-regulating excitatory amino acid carrier 1 (EAAC1). *J Biol Chem*. 2015;290(33):20233–44.
34. Zerangue N, Kavanaugh MP. Interaction of L-cysteine with a human excitatory amino acid transporter. *J Physiol*. 1996;493(Pt 2):419–23.
35. Chen Y, Swanson RA. The glutamate transporters EAAT2 and EAAT3 mediate cysteine uptake in cortical neuron cultures. *J Neurochem*. 2003;84(6):1332–9.
36. Griffith OW. Biologic and pharmacologic regulation of mammalian glutathione synthesis. *Free Radic Biol Med*. 1999;27(9–10):922–35.
37. Rossi DJ, Oshima T, Attwell D. Glutamate release in severe brain ischaemia is mainly by reversed uptake. *Nature*. 2000;403(6767):316–21.
38. Gebhardt C, Korner R, Heinemann U. Delayed anoxic depolarizations in hippocampal neurons of mice lacking the excitatory amino acid carrier 1. *J Cereb Blood Flow Metab*. 2002;22(5):569–75.
39. Dickel DE, Veenstra-VanderWeele J, Cox NJ, Wu X, Fischer DJ, Van Etten-Lee M, Himle JA, Leventhal BL, Cook EH Jr, Hanna GL. Association testing of the positional and functional candidate gene *SLC1A1/EAAC1* in early-onset obsessive-compulsive disorder. *Arch Gen Psychiatry*. 2006;63:778–85.
40. Delgado-Acevedo C, Estay SF, Radke AK, Sengupta A, Escobar AP, Henriquez-Belmar F, Reyes CA, Haro-Acuna V, Utreras E, Sotomayor-Zarate R, Cho A, Wendland JR, Kulkarni AB, Holmes A, Murphy DL, Chavez AE, Moya PR. Behavioral and synaptic alterations relevant to obsessive-compulsive disorder in mice with increased EAAT3 expression. *Neuropsychopharmacology*. 2019;44:1163–73.
41. Wendland JR, Moya PR, Timpano KR, Anavitarte AP, Kruse MR, Wheaton MG, Ren-Patterson RF, Murphy DL. A haplotype containing quantitative trait loci for *SLC1A1* gene expression and its association with obsessive-compulsive disorder. *Arch Gen Psychiatry*. 2009;66:408–16.
42. Fang H, Zhang LF, Meng FT, Du X, Zhou JN. Acute hypoxia promote the phosphorylation of tau via ERK pathway. *Neurosci Lett*. 2010;474(3):173–7.
43. Hervouet E, Cizkova A, Demont J, Vojtkiskova A, Pecina P, Franssen-van Hal NL, Keijer J, Simonnet H, Ivanek R, Kmoch S, et al. HIF and reactive oxygen species regulate oxidative phosphorylation in cancer. *Carcinogenesis*. 2008;29(8):1528–37.
44. Battaglia V, Compagnone A, Bandino A, Bragadin M, Rossi CA, Zanetti F, Colombatto S, Grillo MA, Toninello A. Cobalt induces oxidative stress in isolated liver mitochondria responsible for permeability transition and intrinsic apoptosis in hepatocyte primary cultures. *Int J Biochem Cell Biol*. 2009;41(3):586–94.
45. Li Y, Lein PJ, Liu C, Bruun DA, Giulivi C, Ford GD, Tewolde T, Ross-Inta C, Ford BD. Neuregulin-1 is neuroprotective in a rat model of organophosphate-induced delayed neuronal injury. *Toxicol Appl Pharmacol*. 2012;262(2):194–204.
46. Xu J, Hu C, Chen S, Shen H, Jiang Q, Huang P, Zhao W. Neuregulin-1 protects mouse cerebellum against oxidative stress and neuroinflammation. *Brain Res*. 2017;1670:32–43.
47. Lee JH, Yoo JY, Kim HB, Yoo HI, Song DY, Min SS, Baik TK, Woo RS. Neuregulin1 attenuates H_2O_2 -induced reductions in EAAC1 protein levels and reduces H_2O_2 -induced oxidative stress. *Neurotox Res*. 2019;35(2):401–9.
48. Woo RS, Lee JH, Kim HS, Baek CH, Song DY, Suh YH, Baik TK. Neuregulin-1 protects against neurotoxicities induced by Swedish amyloid precursor protein via the ErbB4 receptor. *Neuroscience*. 2012;202:413–23.
49. Dawson HN, Ferreira A, Eyster MV, Ghoshal N, Binder LI, Vitek MP. Inhibition of neuronal maturation in primary hippocampal neurons from tau deficient mice. *J Cell Sci*. 2001;114(Pt 6):1179–87.
50. Takei Y, Teng J, Harada A, Hirokawa N. Defects in axonal elongation and neuronal migration in mice with disrupted tau and map1b genes. *J Cell Biol*. 2000;150(5):989–1000.
51. Fang B, Zhao Q, Ling W, Zhang Y, Ou M. Hypoxia induces HT-22 neuronal cell death via Orai1/CDK5 pathway-mediated Tau hyperphosphorylation. *Am J Transl Res*. 2019;11(12):7591–603.

52. Pluta R, Ulamek-Kozioł M, Januszewski S, Czuczwar SJ. Shared genomic and proteomic contribution of amyloid and Tau protein characteristic of Alzheimer's disease to brain ischemia. *Int J Mol Sci.* 2020;21:3186.
53. Lewen A, Matz P, Chan PH. Free radical pathways in CNS injury. *J Neurotrauma.* 2000;17(10):871–90.
54. Maiti P, Singh SB, Sharma AK, Muthuraju S, Banerjee PK, Ilavazhagan G. Hypobaric hypoxia induces oxidative stress in rat brain. *Neurochem Int.* 2006;49(8):709–16.
55. Ramanathan L, Gozal D, Siegel JM. Antioxidant responses to chronic hypoxia in the rat cerebellum and pons. *J Neurochem.* 2005;93(1):47–52.
56. Coimbra-Costa D, Alva N, Duran M, Carbonell T, Rama R. Oxidative stress and apoptosis after acute respiratory hypoxia and reoxygenation in rat brain. *Redox Biol.* 2017;12:216–25.
57. Finkel T, Holbrook NJ. Oxidants, oxidative stress and the biology of ageing. *Nature.* 2000;408(6809):239–47.
58. DeGracia DJ, Kumar R, Owen CR, Krause GS, White BC. Molecular pathways of protein synthesis inhibition during brain reperfusion: implications for neuronal survival or death. *J Cereb Blood Flow Metab.* 2002;22(2):127–41.
59. Wang X, Zhang J, Kim HP, Wang Y, Choi AM, Ryter SW. Bcl-XL disrupts death-inducing signal complex formation in plasma membrane induced by hypoxia/reoxygenation. *FASEB J.* 2004;18(15):1826–33.

Publisher's Note

Springer Nature remains neutral with regard to jurisdictional claims in published maps and institutional affiliations.

Ready to submit your research? Choose BMC and benefit from:

- fast, convenient online submission
- thorough peer review by experienced researchers in your field
- rapid publication on acceptance
- support for research data, including large and complex data types
- gold Open Access which fosters wider collaboration and increased citations
- maximum visibility for your research: over 100M website views per year

At BMC, research is always in progress.

Learn more biomedcentral.com/submissions

